Substituting these values in Eq. (5), we have

$$(\nu+\epsilon_{r\phi}) = \frac{U|\partial W/\partial Z|}{\partial^2 W/\partial Z^2} = \frac{U\cdot f(r)\cdot F'(Z/D)\cdot e^{F(Z/D)}}{f(r)[F'(Z/D)]^2\cdot e^{F(Z/D)}}$$

$$= \frac{U}{|F'(Z/D)|} \tag{13}$$

If $F(Z/D)$ is of the form $B(Z/D)$, where B is constant, we have from Eq. (13),

$$(\nu+\epsilon_{r\phi}) = (U\cdot D)/B \tag{14}$$

Then, for a given value of D (or D_H, as the case may be)

$$(\nu+\epsilon_{r\phi}) \propto U \tag{15}$$

This relation shows that $\epsilon_{r\phi}$, is no longer constant in a swirling flowfield, but that it varies directly as the axial velocity U. At the wall, where $U=0$, the eddy viscosity vanishes. This expression for $\epsilon_{r\phi}$ is independent of velocity derivatives and it will therefore never attain values of either zero or infinity as may happen when it is expressed in terms of the velocity derivatives.[4]

Equation (14) is simple, and, using this, the eddy viscosity ($\epsilon_{r\phi}$) can be evaluated from measured mean values of the axial velocities, provided that the constant B is evaluated. This constant can be evaluated by plotting the decay of swirl velocities against (Z/D).

References

[1] Alimov, R. Z., "Certain Characteristics of Transpiration Cooling by a Swirling Flow," *High Temperature*, Vol. 4, 1966, pp. 233-236.

[2] Kreith, F. and Sonju, O. K., "The Decay of Turbulent Swirl in a Pipe," *Journal of Fluid Mechanics*, Vol. 22, 1965, pp. 257-271.

[3] Rochinio, A. and Lavan, Z., "Analytical Investigation of Incompressible Turbulent Swirling Flow in Stationary Ducts," *Journal of Applied Mechanics, Transactions of ASME*, Ser. E, Vol. 36, June 1969, pp. 151-158.

[4] Scott, C. J. and Rask, D. R., "Turbulent Viscosities for Swirling Flow in a Stationary Annulus," *Journal of Fluid Engineering, Transactions of ASME*, Vol. 95, Dec. 1973, pp. 557-566.

[5] Scott, C. J., "A Series Solution for Decay of Swirl in an Annulus," *Journal of Applied Mechanics, Transactions of ASME*, Ser. E, Vol. 39, March 1972, pp. 289-290.

[6] Rao, V. K., Narayanaswamy, K. and Dey, J., "A New Type of Annular Combustion Chamber," *Proceedings of the Third National Conference on I.C. Engines & Combustion*, University of Roorkee, India, Dec. 1976, pp. 319-325.

[7] Wolf, L., Jr., Lavan, Z., and Fejer, A. A., "Measurements of the Decay of Swirl in Turbulent Flow," *AIAA Journal*, Vol. 7, May 1969, pp. 971-973.

[8] Senoo, Y and Nagata, T., "Swirl Flow in Long Pipe, with Different Roughness," *Bulletin of the JSME*, Vol. 15, 1972, pp. 1514-1521.

Tunnel Interference Assessment by Boundary Measurements

C. F. Lo*

ARO, Inc., Arnold Air Force Station, Tenn.

Introduction

A NEW approach to assess and correct wind tunnel interference is urgently needed because of the limitation of the classical theory. The classical method[1] requires a definition of the tunnel wall boundary condition and a mathematical model of the test article. The definition of the wall condition is one of the obstacles to the routine application of classical wind tunnel theory to ventilated transonic wall tunnels.[2] Furthermore, the representation of the test model by certain combinations of singularities neglects all viscous effects. Contrary to the classical approach, a new proposed method, which attempts to avoid these difficulties, requires only the measurement of flow variables at a control surface near the tunnel wall inside the test section. The objective of this Note is to present the new approach and the related derivation of the interference flowfield based on measurements at the control surface. Experimental verification of the new concept is also included.

Received Oct. 25, 1977; revision received Nov. 23, 1977.

Index categories: Testing, Flight and Ground; Subsonic Flow; Transonic Flow.

*Supervisor, PWT/4T Analysis Section, AEDC Division. Member AIAA.

Formulation

A two-dimensional example is chosen to illustrate the formulation of the computation procedure. The Fourier transform technique is applied to the subsonic flow case to obtain the interference flowfield and the flow variables under free-air conditions at the control surface.

The boundary value problem shown in Fig. 1 is formulated to simulate a wind tunnel experiment including measured boundary values (flow variables) at a selected control surface near the tunnel wall, in addition to the regularly measured quantities on the test article. A functional relationship between flow perturbation variables $U_T(x,h)$, $V_T(x,h)$ at the control surface and the model geometry can be obtained by the Fourier transform technique in the transformed plane as follows:

$$\bar{V}_T(p,h) = i\beta\frac{p}{|p|}\bar{U}_T(p.h)\tanh(|p|\beta h) + \bar{F}(p)\cdot\mathrm{sech}(p\beta h) \tag{1}$$

where

$$\bar{F}(p) = (2\pi)^{-1/2}\int_{-\infty}^{\infty} F_x(x)e^{ipx}dx$$

and p is the Fourier transform parameter. The model geometry F should be interpreted as a "potential equivalent" airfoil profile including viscous effects. It is reasonable to assume that the same equivalent profile exists in a free-air flow condition. The solution for free-air flow is readily obtained in the transformed plane

$$\bar{U}_{\text{free air}} = i\frac{p}{\beta|p|}\bar{F}(p)e^{-|p|\beta h} \tag{2a}$$

$$\bar{V}_{\text{free air}} = \bar{F}(p)e^{-|p|\beta h} \tag{2b}$$

Combining Eqs. (1) and (2) to eliminate the model geometry F one obtains the free-air flowfield directly related to the measured tunnel flow perturbation variables U_T, V_T at the control surface without explicit terms of the model geometry.

$$\bar{U}_{\text{free air}} = e^{-|p|\beta h}\left(\bar{U}_T\sinh|p|\beta h + \bar{V}_T\frac{ip}{\beta|p|}\cosh p\beta h\right) \tag{3a}$$

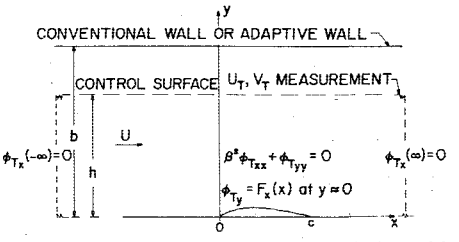

Fig. 1 Boundary-value problem of tunnel simulation with boundary measurements.

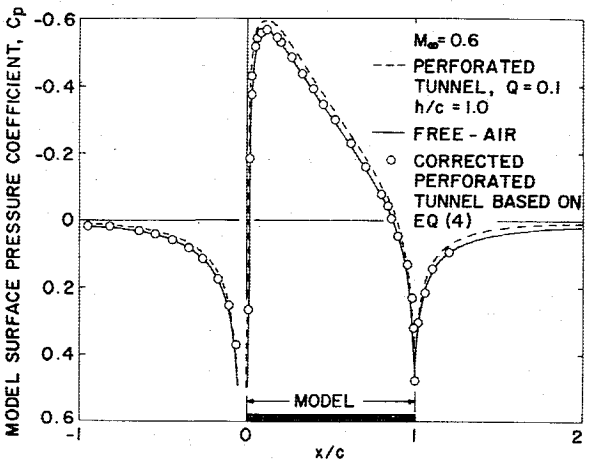

Fig. 2 Numerical verification of interference correction on an NACA 0012 airfoil.

$$\bar{V}_{\text{free air}} = -e^{-ip|\beta h}\left(\bar{U}_T i\beta \frac{p}{|p|}\sinh|p|\beta h - \bar{V}_T \cosh p\beta h\right) \quad (3b)$$

Based on the relationship of Eq. (3) in the physical plane, one can adjust an adaptive-wall wind tunnel to achieve unconfined flow in a single adjustment for subsonic flow without boundary-layer separation on the airfoil.[3] In this Note, Eq. (3) is used to define the interference flowfield by specifying the difference of velocity components between measured tunnel and free-air conditions at the control surface as the boundary conditions. The boundary-value problem which can be solved by the Fourier transform gives the streamwise interference velocity component:

$$U_{\text{int}} = U_T - U_{\text{free air}} = \frac{\beta h}{\pi}\int_{-\infty}^{\infty}\frac{U_T(\xi,h)}{(\beta h)^2+(\xi-x)^2}\,d\xi$$

$$+\frac{1}{\beta\pi}\int_{-\infty}^{\infty}\frac{V_T(\xi,h)(\xi-x)}{(\beta h)^2+(\xi-x)^2}\,d\xi \quad (4)$$

Equation (4) indicates that the interference velocity component is expressed solely in terms of the measured two variables at the control surface. Hence, the interference pressure coefficient is also obtained by $C_{P_{\text{int}}} = -2U_{\text{int}}$. It should be noted that the present method is limited to subcritical flows. Two examples of subcritical flow are given in the following.

Numerical Demonstration

To validate the method, a numerical demonstration is performed by simulating the flow in a wind tunnel with the inviscid, transonic small-disturbance equation. The transonic airfoil program TSFOIL developed by Murman et al.[4] is used to simulate the flow about an NACA 0012 airfoil at $M = 0.6$ in a perforated tunnel with a perforated parameter, $Q = 0.1$ and tunnel semi-height-to-chord ratio, $h/c = 1.0$. By selecting the control surface on the tunnel wall, distributions $U_T(x,h)$ and, $V_T(x,h)$ are substituted into Eq. (4) to determine the interference pressure at the model plane. The tunnel data with the correction from Eq. (4) give excellent agreement with free-air flow results as shown in Fig. 2.

Experimental Verification

A two-dimensional 15.24-cm (6-in) chord NACA 0012 airfoil was tested in the AEDC Aerodynamic Wind Tunnel 1T to verify the present theory. The model is a 6% blockage airfoil spanning the width of the tunnel. The tunnel test section configuration consists of variable perforated walls for the top and bottom walls and solid plexiglass sidewalls, as shown in Fig. 3. Pressure measurements on the airfoil were

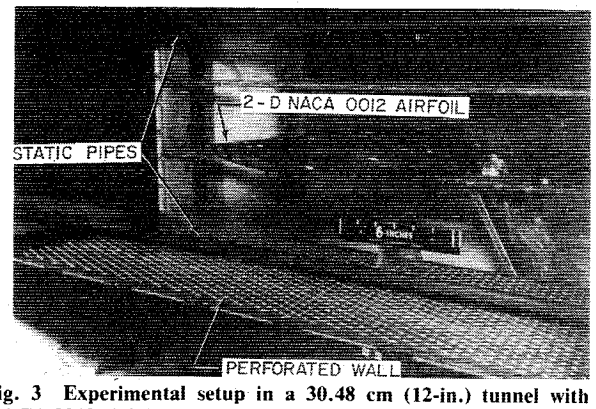

Fig. 3 Experimental setup in a 30.48 cm (12-in.) tunnel with an NACA 0012 airfoil and two state pipes.

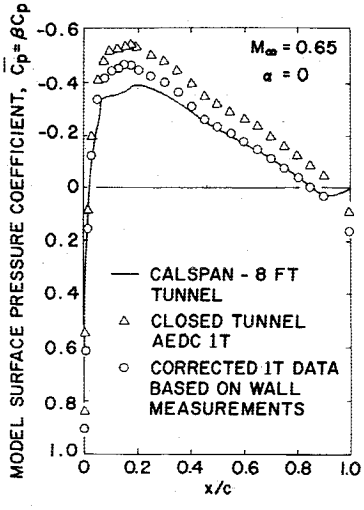

Fig. 4 Experimental demonstration of interference correction on a 6% blockage NACA 0012 airfoil.

obtained along with pressure data from static pipes near the top and bottom walls. The flow angles near the walls were also measured. The data presented in Fig. 4 were obtained for a zero porosity (closed-wall) configuration at $M = 0.65$, which is a subcritical flow. The flow angles at the wall nearly vanish for the closed-wall case and, hence, Eq. (4) approximates to the first term only. The correction to the tunnel data by applying Eq. (4) with the boundary pressure measurements shown in Fig. 4 indicates excellent agreement with interference-free data obtained from Calspan's 8-ft tunnel.[5] The results clearly demonstrate that the new approach for tunnel interference assessment is very promising and requires only a knowledge of flow characteristics at a selected control surface and avoids the difficulties of modeling the test article and tunnel boundary definition.

Acknowledgments

The research reported herein was performed by the Arnold Engineering Development Center, Air Force Systems Command. Work and analysis for this research were done by personnel of ARO, Inc., a Sverdrup Corporation Company, operating contractor of AEDC. Further reproduction is authorized to satisfy needs of the U.S. Government. The contribution of W. L. Sickles on the numerical computation and J. L. Jacocks on the experimental program is greatly appreciated.

References

[1] Pindzola, M. and Lo, C. F., "Boundary Interference at Subsonic Speeds in Wind Tunnels with Ventilated Walls," Arnold Engineering Development Center, Tenn., AEDC-TR-69-47, May 1969.

[2] Jacocks, J. L., "Aerodynamic Characteristics of Perforated Walls for Transonic Wind Tunnels," Arnold Engineering Development Center, Tenn., AEDC-TR-77-61, June 1977.

[3] Lo, C. F. and Kraft, E. M., "Convergence of the Adaptive-Wall Wind Tunnel," *AIAA Journal*, Vol. 16, Jan. 1978, pp. 67-72.
[4] Murman, E. M., Bailey, F. R., and Johnson, M. L., "TSFOIL-A Computer Code for Two-Dimensional Transonic Calculation, Including Wind-Tunnel Wall Effects, and Wave-Drag Evaluation," NASA SP-347, March 1975, pp. 769-788.
[5] Vidal, R. J., Catlin, P. A., and Chudyk, D. W., "Two-Dimensional Subsonic Experiments with an NACA 0012 Airfoil," Calspan Rept. No. RK-5070-A-3, Dec. 1973.

Comparative Study of Fatigue Crack Closure

J. E. Rueping,* B. M. Hillberry,† S. C. Mettler,* and W. H. Stevenson†
Purdue University, West Lafayette, Ind.

Introduction

ONE of the more widely studied concepts for describing fatigue crack growth is the "crack closure" concept advanced by Elber.[1] According to this concept, the crack remains closed over a portion of the tensile part of the load cycle and the crack can propagate only during that portion of the load cycle in which the crack is open. The difference between the maximum applied load and the load at which the crack opens then is considered to be an effective load, which is responsible for advancing the crack. In terms of the stress intensity at the tip of the crack, this becomes

$$\Delta K_{\text{eff}} = K_{\max} - K_{\text{op}} \tag{1}$$

where

ΔK_{eff} = effective stress intensity range
$K_{\max}$ = maximum stress intensity
K_{op} = opening stress intensity

Elber measured the displacement at the edge of the crack during loading with a very sensitive displacement gage and determined the crack opening load by analyzing the nonlinearities of the resulting load vs crack edge displacement curve. The resulting crack opening load is determined from a tangency point on the load vs crack edge displacement curve.

In this investigation, two different techniques were used to measure the crack edge displacements and resulting crack opening loads for constant-amplitude loading with four different stress ratios. In addition, one of the methods was used to measure the crack opening load following an overload/underload type of loading sequence. These results were compared with an inverse method.

Crack Opening Measurement

Many of the experimental investigations of fatigue crack closure have utilized crack edge displacement measurements to obtain the load-displacement curves from which the opening load can be determined. Other methods include the electrical potential method[2-4] and ultrasonic measurements.[5] Edge crack displacement measurements have been made using foil strain gages straddling the crack and bonded only at the ends at the gage.[6] Very sensitive strain gage extensometers using geometries with high strain concentrations have been used for crack edge displacement measurements.[1,7,8]

Pitoniak et al.[9] used an interferometry method to obtain the complete three-dimensional crack surface displacement field in transparent polymethylmethacrylate. Successive photomicrographs were used by Adams[10] to measure crack edge displacements. In this study, crack edge displacement measurements, to determine crack closure behavior, were made using both a strain gage extensometer and a specially developed laser interferometric technique. The laser interferometric technique developed in this study was similar to that used by Sharpe and Grandt.[11] With this system, two horizontal indentations are made on either side of the crack tip using a wedge-shaped diamond indentor. When the two grooves are illuminated by monochromatic light, two interference, or fringe, patterns are formed in space, one above and one below the crack. As the grooves are displaced relative to each other, the fringe patterns move in space. The fringe pattern is focused with a cylindrical lens and transmitted to a phototransistor detector. As the specimen is loaded, the displacements of the grooves cause the fringes to move past a detection slit in front of each of the phototransistors. Calibration is determined from the wavelength of the light emitted from the laser.

If the fatigue crack propagation is described by the effective stress intensity range ΔK_{eff}, as given by Eq. (1), then an inverse technique[12] can be used to determine K_{op} when it varies with geometry or as a result of a load variation. This assumes that ΔK_{eff} establishes the crack growth rate. If the growth rate under steady, constant-amplitude loading conditions is known and can be described as a function of ΔK_{eff}, then, for varying conditions, measuring the growth rate determines the value of ΔK_{eff} which must be advancing the crack under that set of loading conditions. By knowing $K_{\max}$ from the given loading conditions, Eq. (1) then can be solved for K_{op}. Alzos et al.[13] used this method to determine the change in K_{op} following overload/underload type of loading sequences.

Experimental Results

Crack closure measurements were made using 2024-T3 aluminum alloy center crack specimens, $559 \times 152 \times 2.5$ mm. All tests were performed at room temperature in laboratory air. The crack growth was measured with a $100\times$ microscope mounted on a measuring traverse. The test frequency was 20 Hz, and the overload and the cycles for crack opening measurements were applied at 0.02 Hz. (A triangle wave was used for the latter.) For the constant-amplitude tests, the load amplitude was held constant. For the overload/underload tests, the stress intensity was held quasiconstant by load-shedding each 5% of crack growth prior to and following the overload/underload sequence.

For each K_{op} measurement with constant-amplitude loading, the Elber gage was mounted near the crack tip and the data recorded for several cycles. The Elber gage then was removed, and the crack opening displacement was measured with the laser system. The narrow column of light was aligned with the indentations made by the Elber gage which resulted in taking the measurement at nearly the same location relative to the crack tip with each of the two methods. Crack growth data also were obtained.

A series of 16 constant-amplitude tests was run to allow comparison of the crack opening load obtained from the Elber gage with that obtained from the laser interferometric system. Four levels of the stress ratio R were used, 0.01, 0.11, 0.22, and 0.33. For each R, four different stress levels were used. Analysis of the a vs N data confirmed that the results were representative.

Elber defined the parameter

$$U = (K_{\max} - K_{\text{op}})/(K_{\max} - K_{\min}) \tag{2}$$

Received March 2, 1977; presented as Paper 77-362 at the AIAA/ASME 18th Structures, Structural Dynamics, and Materials Conference, San Diego, Calif., March 21-23, 1977; revision received Dec. 27, 1977.

Index category: Structural Durability (including Fatigue and Fracture).

*Graduate Research Assistant.
†Professor.